Axial Segregation of a Settling Suspension in a Rotating Cylinder

Jonghoon Lee* and Anthony J. C. Ladd†

Chemical Engineering Department, University of Florida, Gainesville, Florida 32611-6005, USA

(Received 21 December 2004; published 21 July 2005)

A rotating suspension of nonbuoyant particles can develop striking inhomogeneities in particle concentration, with regular bands of high and low concentration along the symmetry axis. We report Stokes-flow simulations showing that the formation of axial bands is correlated with an inhomogeneous particle distribution in the radial plane. An order parameter, based on the average angular velocity of the particles, characterizes two distinct phases: a low-frequency segregated phase and a high-frequency dispersed phase. The axial band structure develops during the transition between these two phases.

DOI: 10.1103/PhysRevLett.95.048001 PACS numbers: 45.70.Qj, 47.15.Gf, 64.75.+g

A dry granular material segregates by size and mass when flowing down an inclined plane [1] or rotating about a horizontal axis [2]. The segregation occurs in a thin mobile surface layer on top of the packed particle bed [3]. Fingering instabilities have also been observed in nearly monodisperse granular flows [4]. The dominant interactions in these systems are inelastic frictional collisions between the particles, but size segregation is also observed in wet granular slurries [5], although here the contacts between particles are lubricated by the interstitial fluid. More recently, band formation has been observed in dilute monodisperse suspensions, where the interactions are long range and fluid mediated [6–8]. In some of these experiments [6,7], the particles aggregated into well separated bands, but in Ref. [8] much weaker variations in particle concentration were observed.

To try to clarify the experimental results for dilute suspensions, we have carried out numerical simulations within the Stokes-flow approximation, where the Reynolds number is identically zero. At low rotational frequencies, the competition between gravity and the viscous drag of the rotating fluid leads to a number of qualitatively distinct nonequilibrium patterns [8]. The simulations show similar patterns, including the formation of axial bands of high and low concentration. However, we did not observe the more pronounced axial segregation seen at higher rotational frequencies, which we suspect is inertial in origin [6]. We have discovered that the mean angular velocity of the particles is an order parameter, which distinguishes between a low-frequency transversally segregated phase and a high-frequency dispersed phase where particles fill the whole volume uniformly. The order parameter is a function of a single dimensionless frequency, $\Omega^* = \Omega d/u_s$, with a characteristic length that is the mean interparticle separation d. Axial banding develops during the transition between segregated and dispersed phases. Simulations in an oscillating gravitational field show that small axial perturbations in particle concentration can be amplified by a fast unhindered settling, where the up current of fluid flows around a relatively dense and inhomogeneous distribution of particles. This suggests a possible mechanism for the formation of axial bands.

The suspensions of interest are in general dilute, with a mean volume fraction of the order of 1%–2%. We therefore calculate the hydrodynamic interactions between particles in the Oseen approximation [9]; $\dot{\mathbf{x}}_i = \xi^{-1}\mathbf{F}_i + \Sigma_{j\neq i}\mathcal{T}(\mathbf{x}_i, \mathbf{x}_j)\cdot\mathbf{F}_j$, where $\xi = 6\pi\eta a$ is the Stokes friction coefficient for a particle of radius a in a fluid of viscosity η. The force $\mathbf{F}_i$ contains gravitational and centrifugal components, while the Coriolis force is neglected, because it is inertial. The Oseen tensor, $\mathcal{T}(\mathbf{x}_i, \mathbf{x}_j)$, is the Green's function for Stokes flow, and enforces a no-slip boundary condition on the surface of the cylinder [9,10]. The long range approximation to the hydrodynamic fields is well justified in the dispersed phases, but is more questionable when the particle phase is highly segregated. Technical details of the simulations are given in Ref. [11].

The experiments in Ref. [8] use glycerin-water mixtures, with kinematic viscosities, ν, ranging from 5–60 mm^2/s. The particle Reynolds number $\mathrm{Re}_p = 2u_s a/\nu$ is always small, from 10^{-3} to 10^{-1}, while for rotation rates up to and including the low-frequency band phase, the Reynolds number characterizing the fluid flow, $\mathrm{Re} = \Omega R^2/\nu$, is in the range 1–10. In this regime the Stokes-flow approximation is valid. However, at the highest frequencies and lowest viscosities, the tube Reynolds number $\mathrm{Re} \sim 100$, while the experiments in Refs. [6,7] have even higher Reynolds numbers, $\mathrm{Re} > 100$. Thus our simulations are most relevant to the low-frequency patterns observed in Ref. [8].

The key parameters characterizing the nonequilibrium pattern formation are the fluid velocity Ωl, the particle settling velocity $u_s = m_B g/\xi$, and the centrifuging velocity $u_c = m_B\Omega^2 l/\xi$; here m_B is the buoyancy corrected mass of the particle and l is a characteristic length, which is discussed below. Thus at low Reynolds number the flow is characterized by the dimensionless ratios $u_s/\Omega l$ and $u_c/\Omega l$. However, under the conditions of the laboratory experiments, the centrifugal forces are relatively weak, with $u_c/\Omega l \sim 10^{-3}$, and thus the low-frequency pattern formation is determined by a single parameter $u_s/\Omega l$. The

particle distributions shown in Fig. 1 are similar to experimental observations [8] at comparable frequencies.

The particle motions leading to the patterns illustrated in Fig. 1 suggest that the time-averaged angular velocity of the particle phase, $\langle\dot{\theta}\rangle = \langle\Sigma_{i=1}^{N}\dot{\theta}_i\rangle/N$, may play the role of an order parameter, distinguishing between the segregated phase, where the particle returns to the sediment layer without crossing the center of the cylinder, and the dispersed phase where the particles make complete rotations. In fact, $Q = \langle\dot{\theta}\rangle/\Omega$ does show a sharp transition, as illustrated in Fig. 2, separating two distinct phases: a low-frequency segregated phase, where $Q \simeq 0$, and a high-frequency dispersed phase, where $Q \simeq 1$. Figures 1(a) and 1(b) correspond to the segregated phase, Fig. 1(c) corresponds to the transition regime, and Fig. 1(d) corresponds to the dispersed phase.

We have already observed that the nonequilibrium pattern formation in this system is controlled by a dimensionless frequency $\Omega l/u_s$; now we wish to identify the characteristic length l. Figure 2(a) shows that the transition frequency separating segregated and dispersed phases increases with mean particle concentration, but is independent of cylinder size. This suggests that the characteristic length is the mean interparticle separation, $d = n^{-1/3}$, where n is the average particle concentration. Figure 2(b) confirms this scaling and shows that the order parameter is a universal function of the reduced frequency $\Omega^* = \Omega d/u_s$.

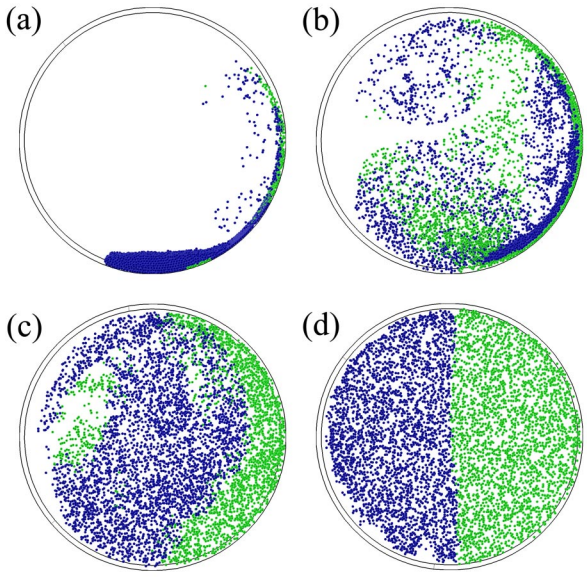

FIG. 1 (color online). Snapshots of the steady-state particle distribution at different frequencies: (a) $\Omega a/u_s = 3.33 \times 10^{-2}$; (b) $\Omega a/u_s = 8.88 \times 10^{-2}$; (c) $\Omega a/u_s = 14.4 \times 10^{-2}$; (d) $\Omega a/u_s = 33.3 \times 10^{-2}$. The average particle volume fraction $\phi = 4\pi na^3/3 \approx 2\%$. The cylinder is rotating counterclockwise and gravity is acting downwards. The green (lighter) particles are moving upwards, while the blue (darker) particles are moving downwards.

A mass balance in the segregated phase supports the selection of the mean interparticle spacing as the characteristic length. At low frequencies, the up flux of particles occurs mainly in the monolayer region next to the cylinder wall [Figs. 1(a) and 1(b)], which lifts particles from the reservoir at the bottom to the upper half of the cylinder with a velocity $\sim\Omega R$. The upward mass flow rate therefore scales as $\dot{M} \sim \Omega RnaL$, where L is the length of the cylinder, and the thickness of the monolayer is taken to be proportional to the particle radius a. The down flux occurs from sedimentation over a cross-sectional area proportional to the cylinder radius: $\dot{M} \sim \bar{u}nRL$. Since the particle distribution is highly inhomogeneous, the up current of displaced fluid does not significantly hinder the particle motion. Consequently, the mean settling velocity, $\bar{u}$, is dominated by hydrodynamic interactions, leading to a higher settling velocity than for individual particles, with a scaling $\bar{u} \sim u_s a/d$. The flux balance is then controlled by

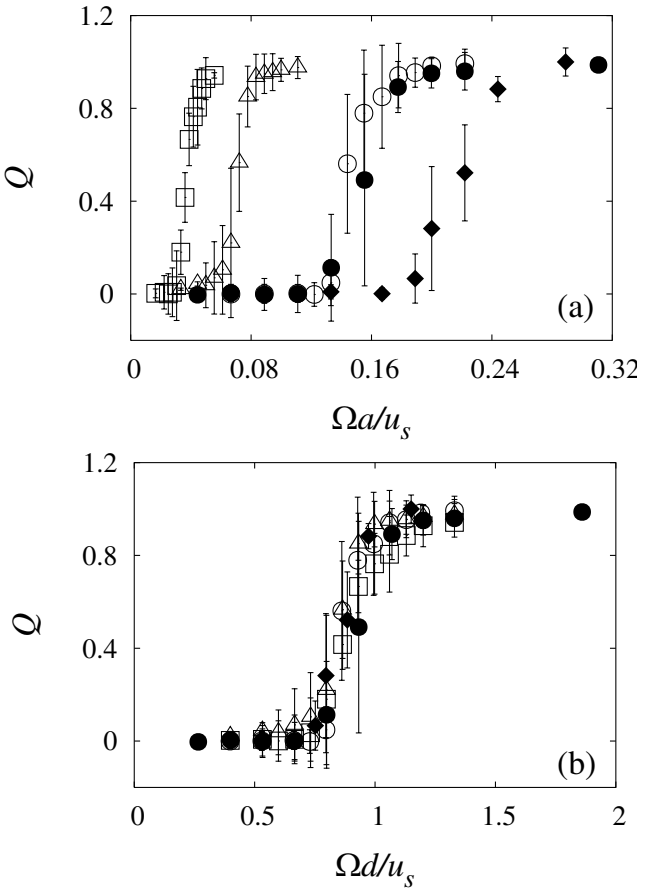

FIG. 2. Rotational order parameter, Q, for different cylinder sizes and particle concentrations; $na^3 = 7.2 \times 10^{-5}$, $R = 100a$ (open squares), $na^3 = 5.8 \times 10^{-4}$, $R = 100a$ (open triangles), $na^3 = 4.7 \times 10^{-3}$, $R = 100a$ (open circles), $na^3 = 4.7 \times 10^{-3}$, $R = 50a$ (closed circles), $na^3 = 9.2 \times 10^{-3}$, $R = 50a$ (closed diamonds). Data are plotted versus the dimensionless frequencies (a) $\Omega a/u_s$ and (b) $\Omega d/u_s$, where $d = n^{-1/3}$. The aspect ratio of the cylinder $L/R = 0.4$.

the dimensionless angular velocity, $\Omega^* = \Omega d/u_s$, in agreement with the simulations.

In the dispersed phase [Fig. 1(d)], the mass balance is different. Now the up flux of particles is distributed over a wider region, proportional to R instead of a, while the hindered settling velocity in the (dilute) dispersed phase is close to that of an isolated particle, u_s. In this case the characteristic dimensionless frequency is $\Omega R/u_s$, and the characteristic length is the cylinder radius R. Thus the transition from segregated to dispersed phases is accompanied by a change in scale of the flow.

The results illustrated in Figs. 1 and 2 were obtained for a short cylinder, $L = 0.4R$, where the suspension is axially homogeneous. For longer cylinders, $L/R \geq 2.0$, the transition is delayed by the onset of axial density fluctuations, and now occurs in the range $0.9 < \Omega^* < 1.4$. The axial band structure emerges during this transition regime. At the low-frequency end of the transition, clusters start to settle through the center of the cylinder, resulting in the growth of axial density perturbations. Empirically we observe that around $\Omega^* = 1$, an axial density perturbation with a well defined wavelength, equal to the cylinder diameter, starts to emerge. As Ω^* increases, the bands become more stable, and around $\Omega^* = 1.3$, we observe a time-independent band structure with a wavelength approximately equal to the cylinder diameter. Figure 3 shows snapshots from a numerical simulation of approximately 12 000 non-Brownian spheres in a cylinder of length $L = 6.2R$, rotating at a reduced frequency $\Omega^* = 1.3$. A coherent pattern of particle density and fluid flow coexist in a nonequilibrium stationary state. The density profile along the cylinder axis is roughly sinusoidal, with a well defined wavelength equal to the cylinder diameter and a magnitude of $0.3n$. Quantitatively similar variations in particle concentration were observed in laboratory experiments under the same conditions [8]. At still higher frequencies, the stability decreases, and bands disappear and reappear with a lifetime of approximately 20 rotations of the cylinder. The magnitude of the density perturbation also decreases at higher Ω^*, leading to a homogeneous distribution of particles over the entire container volume around $\Omega^* \approx 1.5$.

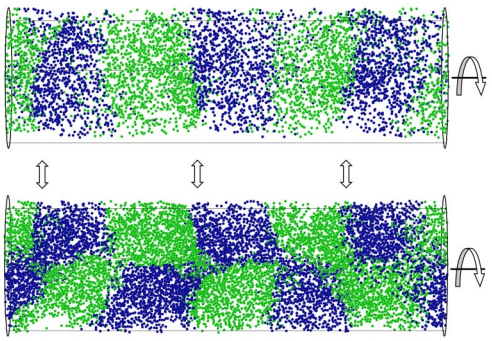

FIG. 3 (color online). Axial bands of high and low concentration in a rotating suspension. The green (lighter) particles are moving to the right, while the blue (darker) particles are moving to the left. Gravity is pointing into the plane of the paper in the upper figure (top view) and downward in the lower figure (front view). The top view of the cylinder shows particles organized into bands with regions of high concentration marked by the arrows. The front view at the same instant shows the generation of secondary axial flows. Particles converge into the high concentration region while settling from the top, and spread out as they reach the bottom wall. The cylinder, length $L = 6.2R$, is rotating at a reduced frequency $\Omega^* = 1.3$. The radius of the cylinder $R = 50a$.

It has long been known that a horizontal line of settling particles is unstable to small perturbations in particle position [12]. Particles slightly closer together than average fall faster, due to the stronger hydrodynamic interaction, drawing more particles towards them and leading to a buckling instability. We propose that axial variations in particle concentration can be amplified by a similar mechanism; the high density regions fall faster, drawing more particles into these regions in a flow that is reminiscent of the classical Rayleigh-Taylor instability. The circular cross section of the vessel plays a crucial role in the development of this instability, diverting the fluid up current away from the settling particles and minimizing hindered settling. By contrast, in a homogeneous suspension the fluid backflow reduces the velocity of the more concentrated regions and stabilizes the suspension. Amplification of axial density fluctuations therefore requires a variation in particle concentration in the radial plane to allow room for the fluid to flow around the particles. Both experiments and numerical simulations show that the axial bands disappear when the particle distribution in the radial plane approaches homogeneity. The proposed mechanism is further supported by simulations with a stationary cylinder and an oscillating gravitational field. When the time period of the gravitational field is similar to the time for a particle to settle the cylinder diameter, we observe bands of high and low concentration, as shown in Fig. 4(a). The wavelength of the bands is again comparable to the cylinder diameter, but the segregation is stronger, leading to dense bands of particles interspersed with pure fluid.

Confinement plays a crucial role in the selection of the dominant wavelength of the axial density perturbations. Screening of the hydrodynamic interactions beyond the cylinder diameter precludes the growth of the density perturbations with wavelengths greater than $2R$. Figure 4(b) shows a simulation where the canceling field from the nonslip boundary condition on the cylinder wall has been neglected. The initial condition was constructed so that the longest wavelength density variation spanned the length of the cylinder. The evolving concentration profile tends to be dominated by the longest wavelength perturbation in the initial condition [Fig. 4(b)], but all wavelengths are unstable and there is no mode selection.

As the rotation frequency increases further, the angular particle distribution becomes more homogeneous and the magnitude of the low-frequency band structure gradually decreases. Around $\Omega^* = 1.5$, a homogeneous distribution over the entire container volume develops and the particle

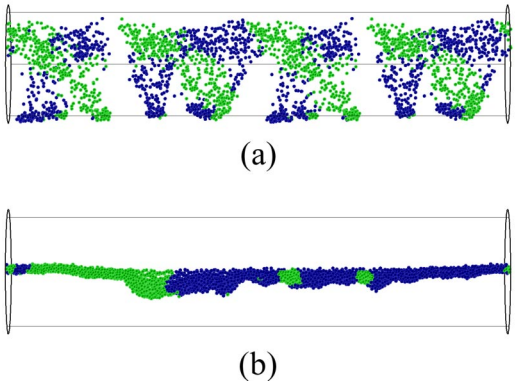

FIG. 4 (color online). Snapshots of the particle distribution generated by an oscillating gravitational field, $g = g_0 \times \sin(\pi u_s t/R)$ in the vertical direction; (a) including the flow field generated by the no-slip boundary condition on the cylinder wall, and (b) excluding the flow field generated by the no-slip boundary condition on the cylinder wall. The green (lighter) particles are moving to the right, while the blue (darker) particles are moving to the left.

phase shows an apparent rigid body rotation with the cylinder [Fig. 1(d)]. In the absence of hydrodynamic interactions, the particles eventually reach a single limiting trajectory bounded by the cylinder wall [13,14], and therefore remain segregated. However, even when the suspension is very dilute, with the particles occupying less than 2% of the total volume, they can be uniformly dispersed throughout the whole vessel by hydrodynamic interactions, as shown in Fig. 1(d). Empirical observations of this dispersed phase led to the development of commercial bioreactors, which utilize this unusual flow to grow cell cultures in a simulated microgravity environment [15]. However, an explanation of how the cells remain dispersed has been lacking.

A detailed examination of the particle motion shows that gravity perturbs the freely rotating trajectory, imposing an additional circular trajectory counter to the flow, with the same period as the rotation of the cylinder, $T = 2\pi/\Omega$, and diameter $u_s T/2 \ll R$. At sufficiently high frequencies the gravitational effects become small and only centrifugal forces remain. We have found that hydrodynamic interactions, even in dilute suspensions, generate a quasidiffusional motion of the particles, which can suppress centrifugal segregation over a limited range of frequencies. We observe only small deviations from uniformity at frequencies $\Omega^* \sim 1.5$.

In an earlier paper we proposed that the axial instability was driven by centrifugal forces [14]. The apparent uniformity of the particle distribution [Fig. 1(c)] led us to erroneously assume that gravitational effects were negligible at these frequencies. The simulations contradict this assumption and show that relatively small regions of pure fluid allow for a substantial reduction in hindered settling, and a gravitationally driven instability to axial density perturbations.

In summary, we have used numerical simulations to investigate the formation of axial bands of high and low concentration in a rotating suspension of nonbuoyant particles. We discovered an order parameter, Q, which characterizes two distinct phases: a low-frequency transversely segregated phase and a high-frequency dispersed phase. We found that the mean interparticle spacing, $d = n^{-1/3}$, is the characteristic length scale at low frequencies, and the dimensionless frequency $\Omega^* = \Omega d/u_s$ governs the transition between the phases. Axial bands are formed during the transition from segregated to dispersed phases. We suggest that angular variations in particle concentration lead to unhindered settling, which amplifies small axial perturbations in particle concentration.

This work was supported by the National Aeronautics and Space Administration, NAG NNCO4GA89G.

*Permanent address: Department of Chemical Engineering, University of California Santa Barbara, Santa Barbara, CA 93106-5080.
†Electronic addresses: ladd@che.ufl.edu; http://ladd.che.ufl.edu

[1] O. Pouliquen, J. Delour, and S. B. Savage, Nature (London) **386**, 816 (1997).
[2] J. M. Ottino and D. V. Khakhar, Annu. Rev. Fluid Mech. **32**, 55 (2000).
[3] O. Zik, D. Levine, S. G. Lipson, S. Shtrikman, and J. Stavans, Phys. Rev. Lett. **73**, 644 (1994).
[4] A. Q. Shen, Phys. Fluids **14**, 462 (2002).
[5] N. Jain, D. V. Khakhar, R. M. Lueptow, and J. M. Ottino, Phys. Rev. Lett. **86**, 3771 (2001).
[6] S. G. Lipson and G. Seiden, Physica (Amsterdam) **314A**, 272 (2002).
[7] A. P. J. Breu, C. A. Kruelle, and I. Rehberg, Europhys. Lett. **62**, 491 (2003).
[8] W. R. Matson, B. J. Ackerson, and P. Tong, Phys. Rev. E **67**, 050301(R) (2003).
[9] J. Happel and H. Brenner, *Low Reynolds Number Hydrodynamics* (Prentice-Hall, Inc., Englewood Cliffs, NJ, 1965).
[10] N. Liron and R. Shahar, J. Fluid Mech. **86**, 727 (1978).
[11] J. Lee, Ph.D. thesis, University of Florida, 2004.
[12] J. M. Crowley, J. Fluid Mech. **45**, 151 (1971).
[13] G. O. Roberts, D. M. Kornfeld, and W. W. Fowlis, J. Fluid Mech. **229**, 555 (1991).
[14] J. Lee and A. J. C. Ladd, Phys. Rev. Lett. **89**, 104301 (2002).
[15] E. A. Botchwey, S. R. Pollack, E. M. Levine, E. D. Johnston, and C. T. Laurencin, J. Biomed. Mater. Res. **69A**, 205 (2004).